Modeling of a Helical Coil Heat Exchanger for Sodium Alanate Based On-board Hydrogen Storage System

Mandhapati Raju[1, 2], Sudarshan Kumar[*, 2]
[1]Optimal CAE Inc.
[2] Chemical Sciences and Material Systems Laboratory, General Motors R&D Center, Warren, MI 48090, USA
*Corresponding author

Abstract: Hydrogen refueling in a metal hydride based automotive hydrogen storage system is an exothermic reaction and therefore an efficient heat exchanger is required to remove the heat for fast refueling. In this paper a helical coil heat exchanger embedded in a sodium alanate bed is modeled using COMSOL. Sodium alanate is present in the shell and the coolant flows through the helical tube. A three-dimensional COMSOL model is developed to simulate the exothermic chemical reactions and heat transfer. Due to memory limitations, only a few turns of the coil are included in the computational domain. Practical difficulties encountered in modeling such three dimensional geometries as well as suitable approximations made to overcome such difficulties are discussed. The distribution of temperature and hydrogen absorbed in the bed for a sample case is presented. A parametric study is conducted using COMSOL-Matlab interface to determine the optimal bed diameter, helical radius and helical pitch for maximum gravimetric capacity.

Keywords: Hydrogen storage, Sodium Alanate, Helical coil heat exchanger, COMSOL.

1. Introduction

Sodium alanate based hydrogen storage systems have received much attention for automotive applications. Sodium alanate has a theoretical hydrogen storage capacity of 5.6% by weight [1-3]. Detailed heat transfer studies for alanate systems using two-dimensional and three dimensional models have been conducted [4, 5] for various bed designs. Previous studies [6] have revealed that the heat exchanger occupies a significant weight and volume of the bed, thereby causing a reduction in the gravimetric and volumetric density of the storage bed. Hence there is a need for designing a compact heat exchanger for fast refueling of the storage bed. In this work, a helical coil heat exchanger is modeled and its performance is evaluated. A three-dimensional COMSOL [7] model has been developed to simulate the refueling of the storage bed. The bed is designed for efficient heat transfer. Alanate is present in the shell and the cooling/heating fluid is passed through the helical tube.

Helical coils are extensively used in industries as heat exchangers and reactors [8, 9] due to many advantages including a comparatively large heat transfer area, high heat transfer coefficient, and small residence time distribution. The heat transfer coefficient is enhanced for flows inside helical passages as compared to flow through straight tubes. Flow through curved passages induces secondary flows causing enhanced convective heat transfer. Several researchers have demonstrated the enhancement of heat transfer coefficient through numerical simulations [10-11] and experiments [12]. Helical coil heat exchangers have also been used for hydrogen storage applications. Various storage concepts and heat exchanger designs, including a helical coil heat exchanger design, have been proposed by Ranong et al. [13] for sodium alanate based hydrogen storage beds. However, detailed modeling of a helical coil heat exchanger has not been reported. Recently, an experimental study has been conducted at Purdue University [14] for a helical coil heat exchanger for $Ti_{1.1}CrMn$, a high pressure metal hydride alloy. The heat exchanger consisted of a $3/8^{th}$ inch helical stainless steel tube with six rings and a helical radius of 39 mm. In our study, focus is on detailed COMSOL modeling of a helical coil heat exchanger for a sodium alanate based hydrogen storage system.

The sodium alanate properties used are for a mixture of sodium hydride, aluminum powder and titanium tri-chloride in a molar ratio of 112:100:4 [3]. The crystalline density and bulk density is based on the values reported by Dedrick et al. [4]. The thermal conductivity of the sample mixture can be increased by addition of thermal conductivity enhancers and thermal conductivity enhancement of up to 8 W/m-K has been reported [4]. In our modeling study, Dexcool™ is used as the cooling/heating fluid. The properties of this cooling fluid are provided

in [15]. During refueling, it is assumed that the station provides the cooling fluid and hydrogen at high pressure. The cooling fluid flowing through the tubes removes the heat of reaction and its flow rate and temperature can be adjusted to enhance the refueling time.

2. Heat Exchanger Design

In this type of heat exchanger design, the shell consists of a cylinder and a helical coiled tube is inserted inside the shell. Alanate is present in the shell and the coolant flows through the helical tube. To simplify the modeling design, only a small diameter vessel with one helical tube placed inside the shell is considered. Hence a multiple number of such vessels may be required for on-board hydrogen storage in a vehicle. Figure 1 shows the schematic of this heat exchanger bed.

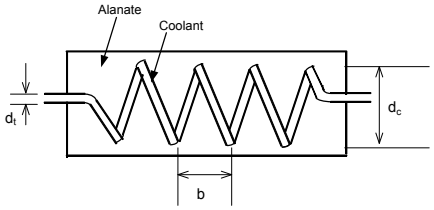

Figure 1. Schematic view of a shell and helical coiled tube heat exchanger

3. Three-Dimensional COMSOL Model for Refueling Simulations

3.1 Computational Domain

Accurate three-dimensional simulation involves constructing the full helical coils consisting of many turns. However due to memory constraints in COMSOL, it is not possible to incorporate the full helical coil in the computational domain. COMSOL is an FEM based multi-physics package and consumes greater random access memory as compared to the other finite volume based computational fluid dynamics packages. To overcome this memory limitation, only a single turn of the helical coil is included. Gas phase convection is neglected and the coupled energy balance and chemical kinetics equations are solved. By assuming periodicity, the computational domain can be approximated to represent the real physical domain.

Even with a single turn of the coil, we encountered other difficulties during the meshing phase due to the complex nature of the geometry itself. Figure 2 shows the preliminary computational domain being chosen. The bed with the helical tube is cut by a horizontal planar surface to include only one turn of the coil. Figure 2 shows the top view and an isometric view of the single coil. The region of intersection with the end planar surfaces with the helical tube is an eccentric ellipse. COMSOL failed to mesh this geometry with tetrahedral mesh due to the presence of eccentric ellipses at the end surfaces.

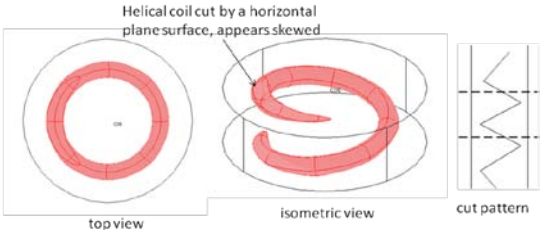

Figure 2. One ring of a helical tube heat exchanger bed obtained by horizontal plane cut

To resolve this problem, we decided to use certain approximations. Four rings of the helical coil are taken and completely enclosed inside the bed as shown in figure 3. Adiabatic boundary conditions are imposed at the ends. The solution near the ends will be quite inaccurate but the solution near the center should be close to the true geometry situation. As shown in figure 3, the computational domain is divided into 3 subdomains by cutting the geometry using two inclined planes. Use of the inclined planes facilitates the numerical solution of this problem. The central subdomain consists of only one helical ring and the solution is considered to be accurate in this region. This assumption is further validated by comparing its solution with a computational domain using six rings. The state of bed is determined by performing an integral average of the quantities in the central subdomain as shown in figure 3.

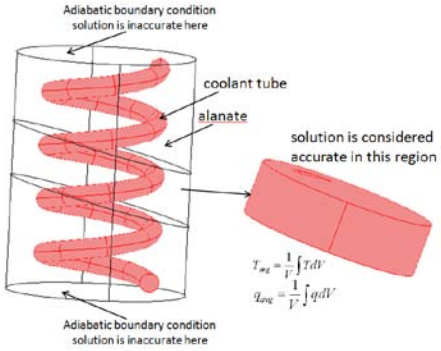

Figure 3. Four rings of a helical tube completely enclosed inside the bed

3.2 Governing Equations

The bed pressure is assumed to be constant through the bed and is equal to the pressure imposed at the inlet of the bed. The tube side heat transfer coefficient is assumed to be constant, and is evaluated based on the cooling fluid flow rate. The gas phase and the bed temperature are assumed to be identical.

Energy equation:

The energy balance for the alanate bed can be written by the following equation:

$$(1-\varepsilon)\rho_{ala}\left(c_p\right)_{ala}\frac{\partial T}{\partial t}=\nabla.\left(k_{ala}\nabla T\right)+Q_a-\varepsilon\rho_g\left(c_p\right)_g\frac{\partial T}{\partial t}+\varepsilon\frac{\partial P_{bed}}{\partial t}-(1-\varepsilon)\rho_{ala}\left(c_p\right)_g q\frac{\partial T}{\partial t} \quad (1)$$

In equation (1), the left hand side is the transient heating of the solid bed, the first term on the right hand side is the heat of conduction term, the second term is the heat of absorption (presented in the next section), the third term is the transient heating of the gas phase, the fourth term is the heat of compression and the last term represents the transient heating of the absorbed hydrogen.

Boundary conditions

Adiabatic conditions are assumed at the outer surface of the cylindrical surface. Convective heat transfer boundary condition $\vec{q}.\hat{n}=h_c A\left(T-T_f\right)$ is applied at the surface of the helical tube which is in contact with the metal hydride bed. The thermal resistance offered by the coolant tube, which is made of aluminum, is neglected.

Thermodynamics and Kinetics

Sodium alanate absorption/desorption kinetics can be described using the following two-step reactions

$$NaAlH_4 \leftrightarrow 1/3Na_3AlH_6 + 2/3Al + H_2 \quad (2)$$

$$1/3Na_3AlH_6 \leftrightarrow NaH + 1/3Al + 1/2H_2 \quad (3)$$

The kinetics model of Luo and Gross [3] is used in the present report. The rate expressions are given as follows.

For $NaAlH_4$ formation:

$$r_{1a}=K_{oa1}\exp\left(-\frac{E_{aa1}}{RT}\right)\ln\left(\frac{P_{bed}}{P_{eq1}}\right)\left(3.9-H\ wt\%\right)^2;\ \left(1.67<H\ wt\%<3.9\right) \quad (4)$$

For Na_3AlH_6 formation:

$$r_{2a}=K_{oa2}\exp\left(-\frac{E_{aa2}}{RT}\right)\ln\left(\frac{P_{bed}}{P_{eq2}}\right)\left(1.67-H\ wt\%\right);\ \left(H\ wt\%<1.67\right) \quad (5)$$

The heat of reaction is given by the expressions below:

$$Q_a=(1-\varepsilon)\rho_{ala}\left(r_{1a}\Delta H_1+r_{2a}\Delta H_2\right) \quad (6)$$

The equilibrium pressures for $NaAlH_4$ and Na_3AlH_6 are given by the van't Hoff expressions

$$\ln P_{eq1}=\frac{\Delta H_1^{'}}{RT}-\frac{\Delta S_1}{R} \quad (7)$$

$$\ln P_{eq2}=\frac{\Delta H_2^{'}}{RT}-\frac{\Delta S_2}{R} \quad (8)$$

The equilibrium and kinetics parameters are presented in Table 1.

Table 1: Kinetic and equilibrium parameters

	K_{oa}	K_{od}	E_{aa} (kJ/mole)	E_{ad} (kJ/mole)	ΔH (J/mole)	ΔS (J/mole-K)
NaAlH4	6.25E+08	1.90E+11	61.6	85.6	-37000	-122
Na3AlH6	1.02E+08	2.90E+10	56.2	88.3	-47000	-126

Heat transfer coefficient

A thorough study of the heat transfer correlations is provided by Mridha and Nigam [9] for flow through helical tubes or curved passages. Considering the range of applicability of the available correlations, the heat transfer correlation by Shchukin [16] closely matches with the current study. This correlation is valid for curvature ratio in the range of [0.01-0.16], Reynolds number in the range of [20000, 67000] and Prandtl number in the range of 7.0. The correlation is given below

$$Nu = 0.0266\left[\frac{\mathrm{Re}^{0.85}}{\lambda^{0.15}} + 0.225\lambda^{1.55}\right]\mathrm{Pr}^{0.4} \quad (9)$$

The Nusselt number for helical coiled tubes (as predicted by eq. 9) is rough 2-3 times higher than that of straight tubes.

4. RESULTS AND DISCUSSION

Results are first provided for a sample case. Later a procedure is described for obtaining the optimal geometry to minimize the heat exchanger weight and volume for a given set of operating conditions. The results from the optimization study are presented subsequently. Table 2 shows the bed geometry for the sample case and the properties of alanate material. The refueling time is chosen as 630 seconds, based on the assumption that only 40% of the DOE refueling rate target is achieved.

Table 2: Bed geometry and properties

Bed diameter (inner)	0.15 m
Cooling tube outer diameter (d_t)	0.016 m
Thickness of the tube	1 mm
Helical pitch	0.045 m
Helical radius	0.045 m
Bulk density	1000 kg/m^3
Porosity	0.48
Specific heat of alanate	1230 J/kg-K
Cooling fluid temperature	380 K
Cooling fluid flow rate	20 LPM
Bed pressure	Ramped up to 150 bar in 360 seconds
Effective thermal conductivity	8.5 W/m-K

Figure 4 shows the contours of the weight fraction of hydrogen absorbed in the bed at 630 seconds. The contours show that the weight fraction is quite uniform across the bed except near the cooling tubes. The weight fractions are unreliable near the bottom and top due to inaccuracy of the solution at the ends. Figure 5 shows the integral averaged quantity of the weight fraction in the central subdomain of figure 3. The weight fraction gradually increases as the hydrogen is getting absorbed in the bed. The kink observed at around 280 seconds is due to the transition from hexahydride formation to the tetrahydride formation. The weight fraction at the end of 630 seconds is 0.0307.

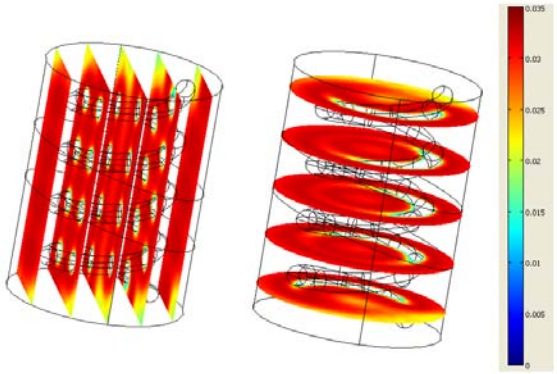

Figure 4. Contours of weight fraction of hydrogen absorbed in the bed at 630 seconds

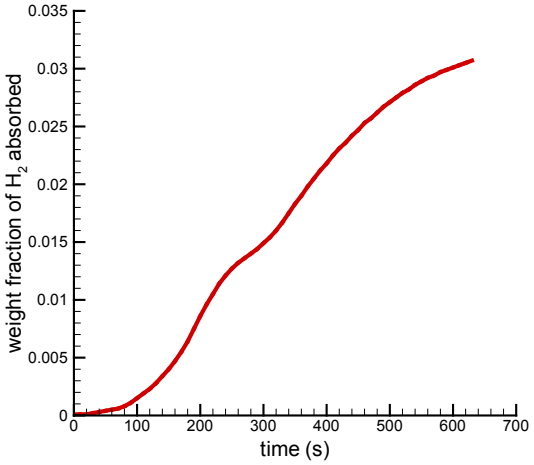

Figure 5. Transient variation of averaged weight fraction of hydrogen absorbed in the bed

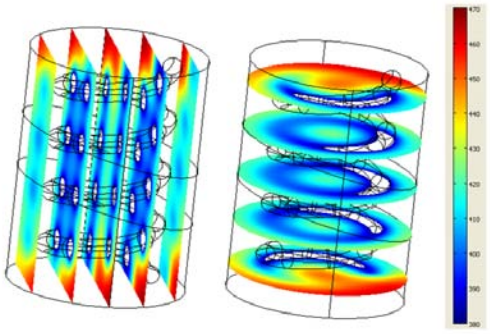

Figure 6. Contours of temperature (K) distribution in the bed

Figure 6 shows the temperature contours in the bed at 630 seconds, corresponding to a 40% fill rate of the DOE 2010 target. The solution at the bottom and top ends is inaccurate as expected. Regions close to the helical coil are at lower temperatures but the temperature is higher along the centerline and at the walls. This is further illustrated in figure 7. Temperature variations along two points - one at the centerline axis and the other at the wall - are shown in red and blue lines respectively. The local temperature, expected to be higher at these locations, should not shoot above the melting temperature of alanate. We observe that the maximum temperature at these locations reaches about 480 K. Figure 7 also shows the integral averaged temperature variation. This temperature is much lower than the temperature at the centerline or at the wall because the temperature near the helical coil is much lower.

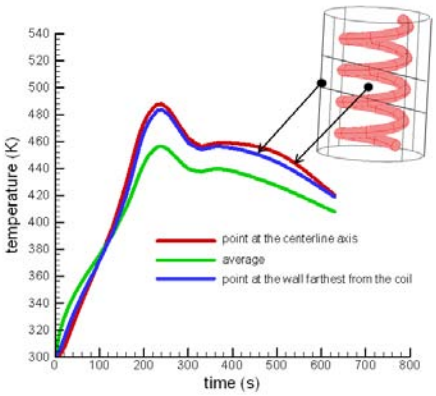

Figure 7. Transient variation of temperature at different locations

To validate the accuracy of the solution, another computational domain consisting of six helical rings is considered. Figure 8 shows the two computational domains consisting of four helical rings and six helical rings. Figure 9 shows the temperature variation along the centerline for both the four helical rings and six helical rings geometries. The two profiles match closely; the two solutions differ by only ~3 K. Figure 9 shows the comparison of the weight fraction of hydrogen absorbed in the bed. The profiles are practically coincident with each other. Based on this observation, the solution resulting from four ring computational geometry can be considered reasonably accurate and is used for all further computations.

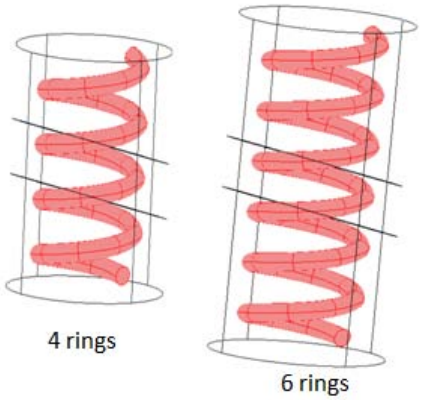

Figure 8. Computational domains including 4 rings and 6 rings respectively

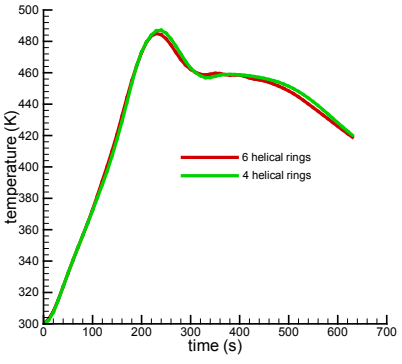

Figure 9. Transient variation of temperature in the centerline region of the domain for 4 helical rings and 6 helical rings

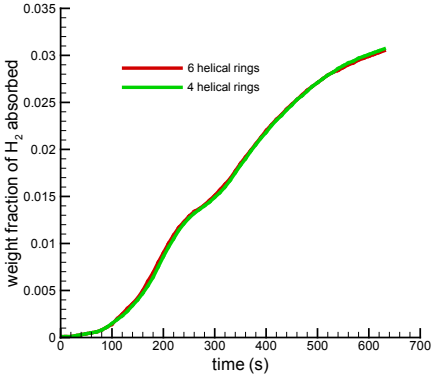

Figure 10. Transient variation of averaged weight fraction of hydrogen absorbed in the bed in the center region of the domain for 4 helical rings and 6 helical rings

5. Optimization of Geometry

The helical coil heat exchanger is optimized in terms of the bed geometry to yield maximum gravimetric capacity for the given operating conditions and properties of the materials. A complete optimization study would involve variation of all the parameters including tube diameter, coolant flow rate, coolant temperature, and operating pressure. This is not within the scope of this study. Our focus is only on the sensitivity to geometric parameters. Cylindrical bed diameter, helical radius and helical pitch are varied systematically. Based on the geometric capacity and the final capacity of the bed at 10.5 minutes, the gravimetric and volumetric capacities are evaluated. Sodium alanate in its tetrahydride phase melts at around 455 K [17] and melting of the alanate causes sintering of the bed which may affect the heat transfer performance of the bed. Previous research [18] has shown that melting does not significantly affect the absorption/desorption characteristics of the alanate, even at temperatures up to 500 K. In our computations, we limit the maximum temperature of the bed to 500 K. If a particular geometry fails this check, it is removed from consideration. Of all the cases that pass this test, the case with the maximum gravimetric capacity is identified.

Table 3 shows the performance of different geometries. The shell radius, helical radius and helical pitch are systematically varied. The performance of each geometry is reported in terms of the amount of hydrogen stored for a 10.5 refueling time normalized for the weight and volume of the bed. The simulations from the COMSOL study gives information of quantities per unit helical ring but the reported results have been scaled to 20 helical rings. Hence the quantities reported in Table 3 are for 20 helical rings with the assumption that each bed would consists of 20 helical rings. A 5 kg usable hydrogen bed would require multiple beds, for example, 8 beds of the first geometry would be necessary. In the calculations reported in Table 3, only the alanate and the heat exchanger weight and volume are considered. The containment vessel, extra space requirements and the balance of plant components are not included in these calculations.

For each case, the maximum temperature (spanning all the points in time and space) observed during refueling is reported. If the maximum temperature rises above 500 K, as shown in red cells in Table 3, then that particular geometry is rejected. For cases 1, 7, and 8, the maximum temperature is < 500 K. Table 3 lists only a partial list of cases that have been examined and shows the set of cases run for the second level of screening to find an optimal geometry. Initial screening was done to find a set of geometric parameters that would give approximately 3% or higher by weight of hydrogen absorption in 10.5 minutes. Cases 1 and 7 achieve maximum system gravimetric and volumetric hydrogen storage capacities (0.0289 kg/kg and 29.3 g/L). However, the maximum temperature for case 1 is lower compared to the maximum temperature observed in case 7. Hence case 1 is a better option compared to case 7. The results show that helical coil heat exchanger is very effective in terms of reducing the weight and volume of the heat exchanger. It was observed [6] that for straight cooling tube interconnected by fins, the weight of the fins and tubes were approximately 30% of the total weight of the bed. For the helical coil heat exchanger, the heat exchanger weight is about 3% of the total weight of the bed. This value would of course be higher when the pressure vessel and other system components are taken into account.

Table 3: Performance of different helical coil heat exchanger geometries

	case-1	case-2	case-3	case-4	case-5	case-6	case-7	case-8
Shell radius (m)	0.075	0.08	0.088	0.01	0.075	0.075	0.075	0.07
Helical radius (m)	0.045	0.05	0.055	0.06	0.05	0.04	0.045	0.04
Helical pitch (m)	0.045	0.05	0.055	0.06	0.045	0.045	0.05	0.04
Weight fraction of H_2 absorbed after 10.5 min	0.0307	0.0306	0.0287	0.025	0.03	0.0293	0.0307	0.03
Maximum temperature (K)	480	512	506	538	506	509	492	473
Mass HEX (20 helical rings) (kg)	0.7285	0.8095	0.8904	0.9714	0.8076	0.6497	0.7306	0.6476
Volume HEX (20 helical rings) (m^3)	1.2E-03	1.3E-03	1.4E-03	1.5E-03	1.3E-03	1.0E-03	1.2E-03	1.0E-03
mass of alanate (20 helical rings) (kg)	24.145	30.700	41.158	58.427	26.765	21.533	24.215	18.564
Volume of alanate (20 helical rings) (m^3)	0.0241	0.0307	0.0412	0.0584	0.0268	0.0215	0.0242	0.0186
Absorbed hydrogen (20 helical rings) (kg)	0.7413	0.9394	1.1812	1.4607	0.8029	0.6309	0.7434	0.5569
Fractional weight of H2 stored per unit weight of bed*	0.0289	0.0290	0.0273	0.0240	0.0283	0.0277	0.0289	0.0282
Weight of H2 stored per unit volume of bed* (g/L)	29.303	29.376	27.751	24.360	28.635	27.967	29.303	28.433
* Includes only the alanate and the heat exchanger, the containment vessel is not included. Hydrogen in the gas phase is not included								

6. Conclusions

Heat transfer and chemical kinetics for a helical coil heat exchanger embedded in a sodium alanate bed can be modeled by using only four helical turns in a three dimensional COMSOL geometry. The helical coil heat exchanger designs considered here are very efficient in achieving good heat transfer rates and offers advantages of low heat exchanger mass and volume. Preliminary estimation of gravimetric capacity shows that an optimized helical coil heat exchanger is significantly better than a heat exchanger involving cooling tubes interconnected with fins in a sodium alanate bed.

7. References

1. Bogdanovic B, Brand R, Marjanovic A, Schwickardi M, Tolle J. Metal-doped sodium aluminum hydrides as potential new hydrogen storage materials. *J Alloys Compd*, **302**, 36-58 (2000).

2. Sandrock G, Gross K, Thomas G. Effect of Ti-catalyst content on the reversible hydrogen storage properties of the sodium alanates. *J Alloys Compounds*, **339**, 229-308 (2002).

3. Luo W, Gross, KJ. A kinetics model of hydrogen absorption and desorption in Ti-doped $NaAlH_4$. *J Alloys Compounds*, **385**, 224-231 (2004).

4. Dedrick DE, Kanouff MP, Larson RS, Johnson TA, Jorgensen SW. Heat and mass transport in metal hydride based hydrogen storage systems. Proceedings of HT 2009, ASME summer heat transfer conference, July 19-23, San Francisco, CA (2009).

5. Hardy BJ and Anton DL, Hierarchical methodology for modeling hydrogen storage systems. Part II: Detailed models, International Journal of Hydrogen Energy, **34**, 2922-3004 (2009).

6. Raju M, Kumar S, System Simulation Modeling and Heat Transfer in Sodium Alanate

Based Hydrogen Storage Systems. Submitted to *International J. Hydrogen Energy*.
7. COMSOL Multiphysics, version 3.5a.
8. Ali S. Pressure drop correlations for flow through regular helical coil tubes. *Fluid Dynamics Research*, **28**(4), 295-310 (2001).
9. Mridha M, Nigam K. Numerical study of turbulent forced convection in coiled flow inverter. *Chemical Engineering and Processing. Process Intensification*, **47**(5), 893-905 (2008).
10. Jayakumar J, Mahajani S, Mandal J, Iyer K, Vijayan P. CFD analysis of single-phase flows inside helically coiled tubes. *Computers & Chemical Engineering*, **34**(4), 430-446 (2010).
11. Wu S, Chen S, Li Y, Li L. Numerical investigation of turbulent flow, heat transfer and entropy generation in a helical coiled tube with larger curvature ratio. *Heat and mass transfer*, **45**(5), 569-578 (2009).
12. Salimpour M. Heat transfer coefficients of shell and coiled tube heat exchangers. *Experimental Thermal and Fluid Science*, 33(2), 203-207 (2009).
13. Ranong C, Höhne M, Franzen J, Hapke J, Fieg G, Dornheim M, Concept, Design and Manufacture of a Prototype Hydrogen Storage Tank Based on Sodium Alanate. *Chemical Engineering & Technology*, **32**(8), 1154-1163 (2009).
14. Visaria M, Mudawar I, Pourpoint T. Experimental Results and Analysis of Coil-in-Coil Heat Exchanger for Hydrogen Storage Using $Ti_{1.1}CrMn$. *GM Internal report*, 2010.
15. Raju M, Ortmann, JP, Kumar S. System Simulation Model for High-Pressure Metal Hydride Hydrogen Storage Systems. *International Journal of Hydrogen Energy*, **35**(16), 8742-8754 (2010).
16. Shchukin VK. Correlation of experimental data on heat transfer in curved pipes, *Thermal Engg.*, **36**, 72-76 (1969).
17. Gross KJ, Guthrie S, and Thomas GJ, In-situ X-ray diffraction study of the decomposition of NaAlH4, *Journal of Alloys and Compounds*, **297**, 270–281 (2000).
18. Gross K, Thomas G, Sandrock G. Hydride development for hydrogen storage, *Proceedings of the 2000 hydrogen program review*, NREL/CP-570-28890.

8. Acknowledgements

This work was performed under DOE contract DE-FC36-09GO19003 as GM's contribution to the DOE Hydrogen Storage Engineering Center of Excellence (HSECoE). The authors would like to acknowledge the support of Ned Stetson, Monterey Gardiner and Jesse Adams of DOE and Don Anton of SRNL. The authors also acknowledge Mei Cai and Scott Jorgensen of General Motors for their valuable suggestions.

9. Nomenclature

A	area of heat transfer, m^2
b	helical pitch, m
$c_{p,ala}$	specific heat of metal hydride bed, J/kg-K
$c_{p,g}$	specific heat of H_2 gas, J/kg-K
d_t	tube diameter, m
d_c	helical coil diameter, m
$c_{p,g}$	specific heat of H_2 gas, J/kg-K
E_{aa1}, E_{ad1}	activation energy of absorption/desorption of reaction 1, J/mole-H_2
E_{aa2}, E_{ad2}	activation energy of absorption/desorption of reaction 2, J/mole-H_2
h_c	heat transfer coefficient in the tube, W/m^2-K
k_{al}, k_{ala}	thermal conductivities of aluminum and alanate, W/m-K
$\vec{n}$	unit normal vector
Nu	Nusselt number
Pr	Prandtl number
P_{bed}	bed pressure, Pa or bar
P_{eq1}	equilibrium pressure of Tet phase, Pa or bars
P_{eq2}	equilibrium pressure of Hex phase, Pa or bars
q	weight fraction of H_2 absorbed in the bed
$\vec{q}$	heat flux at the tube surface
Q_a	Heat of absorption, J/kg-K
Re	Reynolds number
r_{1a}, r_{1d}	rate of absorption/desorption from reaction 1, 1/hr
r_{2a}, r_{2d}	rate of absorption/desorption from reaction 2, 1/hr
T	temperature, K
T_f	cooling fluid temperature, K
t	time, s
U	overall heat transfer coefficient, W/m^2-K
ε	porosity
ρ_{ala}	density of alanate, kg/m^3
ΔH	heat of absorption, J/kg
$\Delta H'$	heat of absorption, J/mole
ΔS	entropy of absorption, J/kg-K
λ	curvature ratio, d_t / d_c